Tech Science Press

Adaptive Nonlinear Sliding Mode Control for DC Power Distribution in Commercial Buildings

R. Muthamil Arasi[1,*] and S. Padma[2]

[1]Thiagarajar Polytechnic College, Salem, Tamilnadu, India
[2]Sona College of Technology, Salem, Tamilnadu, India
*Corresponding Author: R. Muthamil Arasi. Email: tptcmuthamizh@gmail.com
Received: 24 May 2022; Accepted: 29 June 2022

Abstract: The developing populace and industrialization power demand prompted the requirement for power generation from elective sources. The desire for this pursuit is solid due to the ever-present common assets of petroleum derivatives and their predominant ecological issues. It is generally acknowledged that sustainable power sources are one of the best answers for the energy emergency. Among these, Photovoltaic (PV) sources have many benefits to bestow a very promising future. If integrated into the existing power distribution infrastructure, the solar source will be more successful, requiring efficient Direct Current (DC)-Alternating Current (AC) conversion. This paper mainly aims to improve controllers' performance between AC/DC Energy sources and the DC loads using the Adaptive Nonlinear Sliding Mode (ANSM) control method. The proposed ANSM method efficiently controls power quality issues, such as transient response, power flow reliability and Total Harmonics Distortion (THD). The proposed controller is applied for both AC/DC and DC/DC converters and the performance of the proposed controller is validated through simulation checking the above parameters. The simulation results confirm ANSM configuration is more reliable and efficient than the existing fuzzy and sliding mode control methods.

Keywords: Photovoltaic; AC-DC converter; DC-DC converter; adaptive nonlinear sliding mode; transient response; total harmonics distortion

1 Introduction

Integrating Renewable Energy Source (RES) with existing power systems are proposed to have better performance and efficiency in handling multiple energy sources with ease of feasible implementation and conservation. Solar panels and wind turbines are examples of renewable energy systems. The concept of using Direct Current (DC) in a building power distribution system arose from the need to take advantage of benefits such as rapid development of Photovoltaic (PV) system installation. R. Mohd et al. 2019 [1], the growing use of batteries in commercial buildings. Rosales-Asensio et al. 2019 [2] and the growing nature of DC loads in the market, such as consumer electronics, gadgets, motor drives, and solid-state lighting systems using Light Emitting Diodes (LEDs). Sundareswaran et al. 2019 [3]. Because the DC

power distribution system in Buildings. Lai et al. 2019 [4] avoids converting solar DC electricity to AC and then back to DC to provide DC loads, energy transfer losses are greatly reduced.

In today's environment, commercial buildings utilize 61 percent of the country's electrical energy Vishwanath et al. 2019 [5], with lighting systems the most common demand. The current power system in business buildings, on the other hand, relies on AC and DC energy from sustainable power sources, which must be converted from DC to AC, then AC to DC to power the DC loads [6,7]. The power transfer efficiency is substantially enhanced when DC power is delivered directly to DC loads through DC Bus. Therefore developing DC distribution systems to adapt to sustainable renewable power sources and DC loads is necessary Kitson et al. 2019 [8]. Tab. 1 depicts the many types of DC loads found in commercial buildings.

Table 1: Various DC loads in commercial buildings

S. No	Different types of DC loads
1	Computer (48 V with 200 W)
2	Automatic gate opening systems (12 V with 100 W)
3	Lighting System (Volt 12 V with 3 W, 5 W, 7 W, 9 W, 15 W, 40 W, 100 W, 500 W and 1000 W)
4	Washer and Dryers (24 V with 750 W, 1000 W and 1500 W)
5	Water purifier (36 V with 20 W, 50 W and 100 W)
6	Elevator (75 V with 2000 W) Television (12 V with 10 W (24 inch), 20 W(32 inch) and 50 W (50 inch) Video audio monitors (12 V with 40 W, 100 W and 250 W)
8	Air cooler (12 V with 36 W, 48 W, 75 W, 125 W and 200 W)
9	Ceiling fans (12 V with 35 W)
10	Mixer grinder (12 V with 600 W)
11	Water heater (24 V with 300 W, 400 W and 500 W)

Fig. 1 shows a model of a 48 V DC solar hybrid distribution system for Indian rural banks. This paper offers a DC distribution system for commercial buildings that includes both AC and DC sources. Pulse Width Modulation (PWM) current and voltage mode control, Proportional Integrated (PI), and Proportional Integrated Derivative (PID) control [9–15] are the most used control techniques for AC to DC and DC to DC converters. Under fluctuating loads and power system conditions, these traditional control techniques do not function well. Under heavy load and power system fluctuation circumstances, the current Nonlinear Sliding Mode Method Rehman, Abdul Ashraf et al. 2018 [16–19] performs adequately, but it does not account for transitory conditions. Therefore, in this work, an Adaptive Nonlinear Sliding Mode method is introduced to accommodate transient and steady-state conditions and performance parameters like peak time, peak overshoot time, recovery time, steady-state error, and THD verified.

2 Proposed Converter Design and Analysis

The functional working diagram of the proposed system is shown in Fig. 2. In this work, Adaptive Nonlinear Sliding Mode (ANSM) Controller is used to control the switching operation of the converters. The power converters connected to the sources and the common DC bus will be controlled under an ANSM. The proposed ANSM control technique generates continuous 380 V DC. Hernández et al.

2018 [20] based on the PV panel and AC supply reference signals. The numerical simulation of this model ensures the accurate operation of the supervisory controller and its algorithm functions in different operating conditions [21–23].
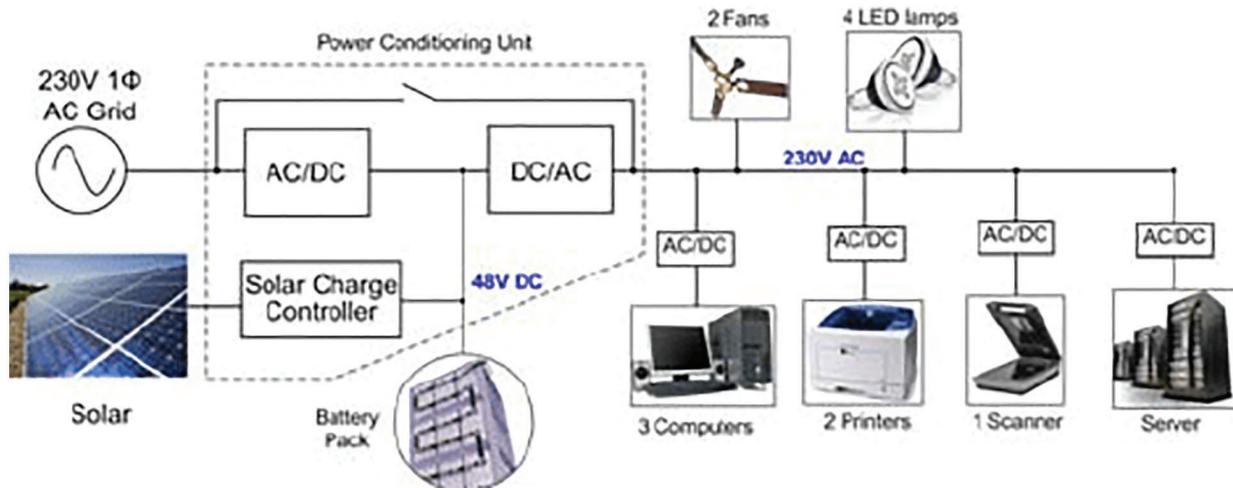
Figure 1: 48 V DC solar hybrid distribution system for Indian rural banks
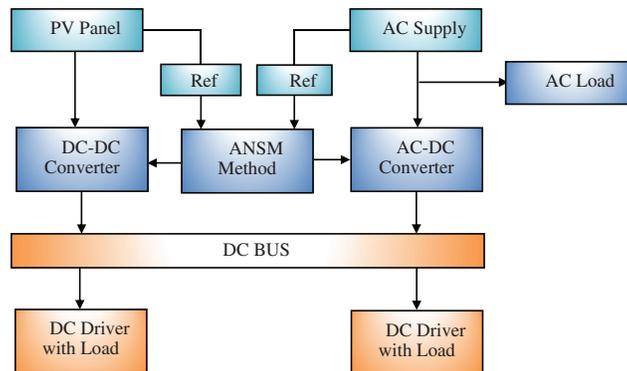
Figure 2: Block diagram of proposed system

2.1 Operation of DC-DC Boost Converter Circuit

Fig. 3 depicts the DC-DC boost converter's circuit diagram. This paper proposes a simpler analysis of a new modulation method for converting boost converters called the ANSM Modulation Scheme. It features two different width trains to mitigate high pulse distortions and reduce power loss in power electronic systems. Single switched PWM DC-DC Boost Converters were employed in the suggested modulation method.

The modulation technique created by this type minimizes high-order synchronization while the narrow region of the wide lentil segment reduces low-order synchronization. Zero number counts the signal and is in ascending and descending stairs. The ascending region is the inverse of the descending region. The amplitude of the voltage signal is equal to the height of the modulating signal.
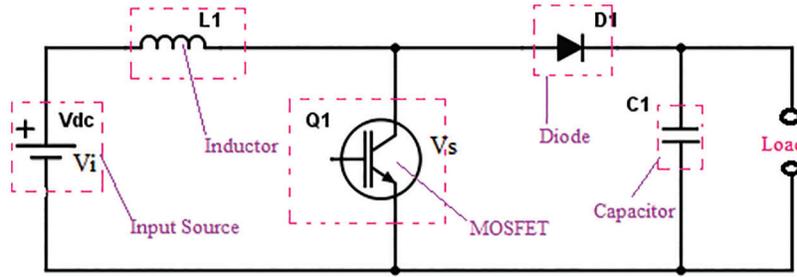
Figure 3: Circuit diagram of boost converter

2.1.1 Modes of Operation for Proposed DC-DC Converter

The function of the DC-DC converter is to be controlled and kept constant under steady-state against variations in input voltage and load. The proposed SMC function is designed to adjust the time-varying proportional area of the step/pulse according to the control of the Adaptive Nonlinear sliding mode.

$$R_S = X_1(t)x(D_\infty - A_o) \tag{1}$$

where,

R_s = Sliding space; D_∞ = Reference Output Voltage; A_o = Obtained output voltage; X_1 = Positive Switching interval

If $X_1(t) > 0$ is the parameter with ANSM time varies according to the constant or change interval. It is properly selected, and the sliding coefficient is modeled to meet the required level of stability. K1 (t) is considered the sequence in which this control system occurs, whose product is zero at any given time. Thus the differential sliding function (2) is expressed.

$$R_s|Q_s = -X_1(t)A_o \tag{2}$$

where: Q_s = trending path

$$A_{eq} = 1 - \frac{A_o}{i_L} \tag{3}$$

Then the corresponding trending law is defined by

$$R_S = -X_1(t)x(D_\infty - A_o) \tag{4}$$

Based on the output track system, the transformation function of the nonlinear sliding mode is computed. When the difference between the reference and actual output voltages is zero, Eq. (6) becomes:

$$d(t) = 1 - \frac{D_i}{D_\infty} \tag{5}$$

The values of the load barrier can be seen well in itself when determining the independent and sliding coefficients of the controller inductor. Accordingly, the converter operates in two different modes-Continuous Current Mode (CCM's) and Discontinuous Current Mode (DCM).

2.1.2 Continuous Current Mode

As shown in Fig. 4, when the duty cycle is such that the inductor current flow is continuous during the entire switching period in both charging as well as discharging timings and the current does not reach zero, it is CCM operation In Fig. 4, D1TS and D2TS are the transition cycles, D1 is the ratio of duty cycle and D2 y = 1-D.
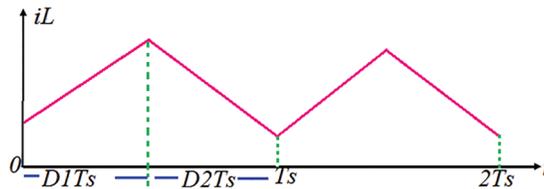
Figure 4: Inductor current response-CCM operation

As shown in Fig. 5, when the duty cycle is such that the inductor current flow is continuous during the entire switching period in both charging as well as discharging timings and the current does cross zero to swing between positive and negative, it is Forced CCM (FCCM) operation
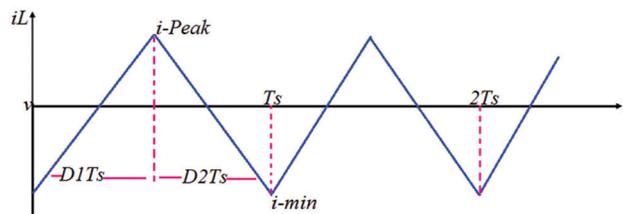
Figure 5: Inductor current-FCCM

The operation of the boost converter CCM, the signal, output voltage fluctuation, diode current, and power inductor current are illustrated in Fig. 6.
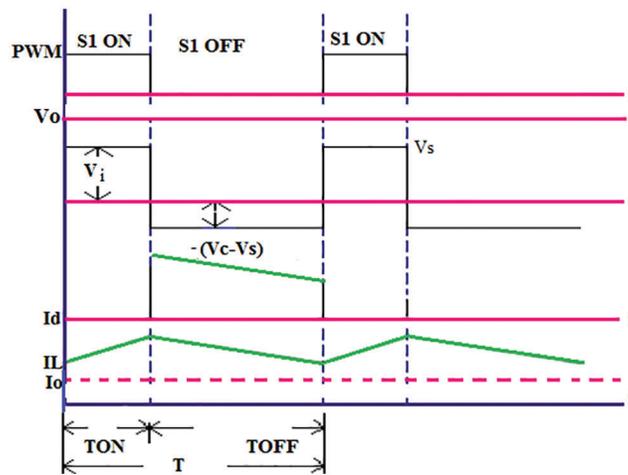
Figure 6: VI Characteristics with time in CCM

2.1.3 Discontinuous Current Mode

If the duty cycle value is selected, the discharging is completed before the end of one time period Ts. The inductor current will reach zero for a small period D3Ts, as shown in Fig. 7.

The operation of DCM is consists of three stages. Here D_1 is the duty cycle, $D_2 = (1-(D_1-D_3))$ and $D_3 = (1-(D_1-D_2))$. During the third interval-D3TS, the current is Zero. The DCM standardized output voltage has no linear relationship with the input voltage as of the CCM. The signal, output voltage variation, diode current and current inductor current in the DCM function of the boost converter is depicted in Fig. 8.
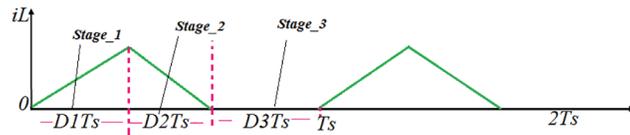
Figure 7: Inductor current response-DCM operation
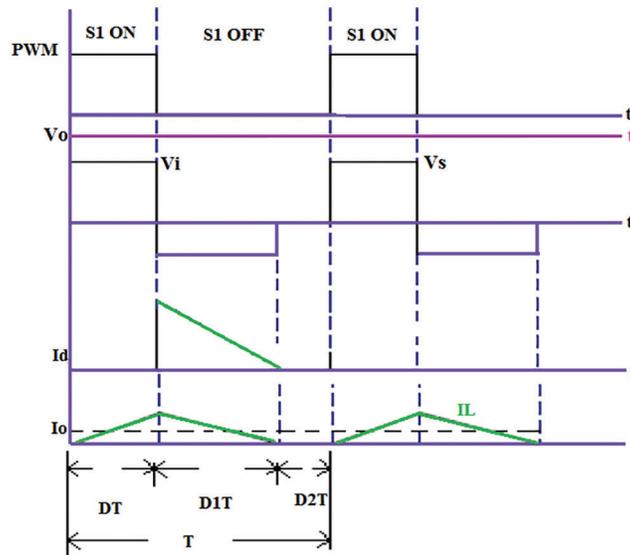
Figure 8: IV characteristics with time in DCM

2.2 Operation of AC-DC Converter

This area depicts the activity of the proposed single-stage AC to DC converter. Fig. 9 shows the proposed block chart for AC-DC converter with an Adaptive Nonlinear sliding Mode Control strategy. The ANSM control strategy gives the ideal outcomes against different boundaries, such as voltage adjustment, unity power factor, and decreasing switching losses.
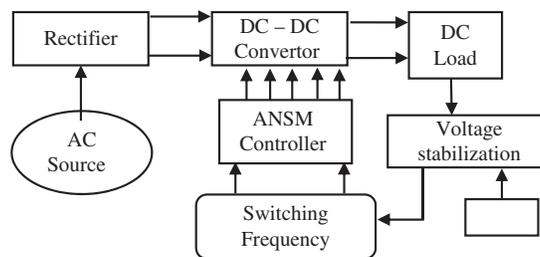
Figure 9: AC-DC Converter-block diagram

2.2.1 Buck-Boost Converter Circuit

The proposed ANSM-based buck-boost converter is shown in Fig. 10, suitable for both step-up and step-down applications. This work obtains step up and step-down output voltage characteristics through a suitable transition scheme by switching power semiconductor switch.
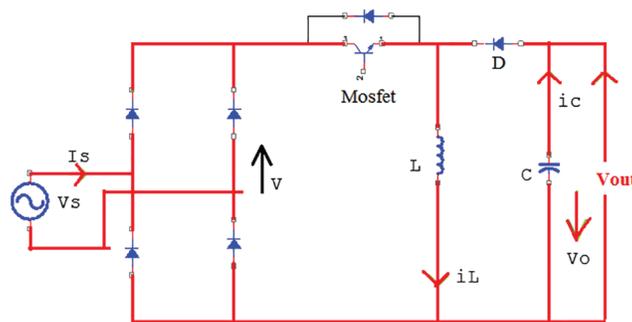
Figure 10: Circuit diagram of buck-boost converter

2.2.2 Modes of Operation

The Buck-Boost Converter operates in three operating modes and each having sub-modes. *Charging mode (mode 1)*

The switching device MOSFET is in charging mode, diode D is in reverse bias, and supply voltage appears across the inductor. As illustrated in Fig. 11, the inductor current should climb towards IL and follow a return path to the AC input side. The charge stored in the capacitor C in the previous Period also drives the inductor through the diode. Green lines in Fig. 11 indicate current paths in the circuits in this mode.
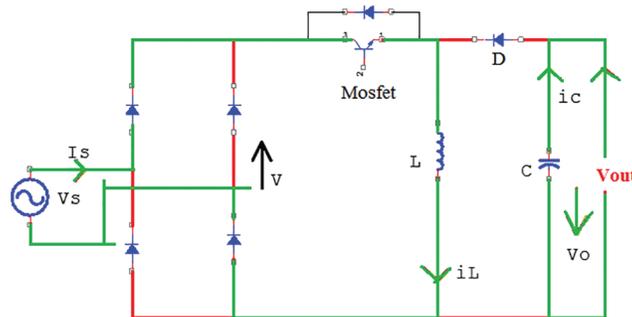
Figure 11: Mode-1 MOSFET-ON and diode DOFF

Discharging mode (mode 2)

The circuit diagram of Mode 2 is shown in Fig. 12. In this mode, the swathing device MOSFET is there in OFF state, Diode D is forward bias, and the output voltage IL drops across inductor IL. Attempting to leave its post passing through a head diode D in anticipation of the voltage load of the inductor changes its peak and burns and charges the capacitor as the requirements remain.
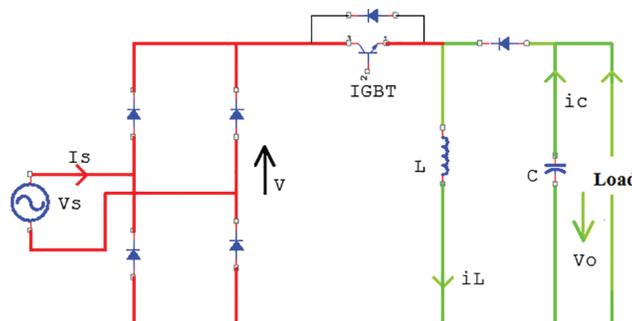
Figure 12: Mode-2 MOSFET-OFF and diode D-ON

Mode 3 (Off Mode)

The circuit diagram of mode3 is shown in Fig. 13. The switching device MOSFET is in the OFF state in this mode. The inductor current IL falls to zero, and the reversing bias diode (D) is activated. The operation of this model continued until the MOSFET turned ON.
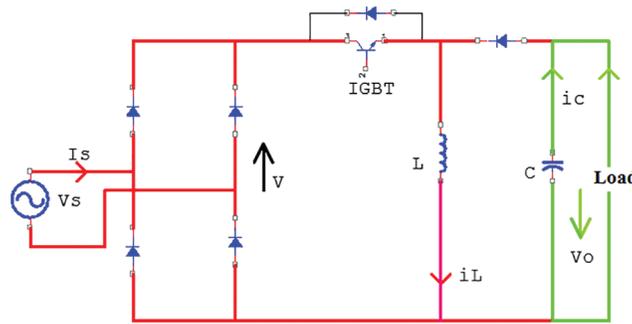
Figure 13: Mode-3 MOSFET is OFF, and diode DOFF

2.2.3 Inductor Current and Voltage Response During One Switching Cycle

Fig. 14 depicts the voltage and current responses in both CCM and DCM during a single switching cycle.
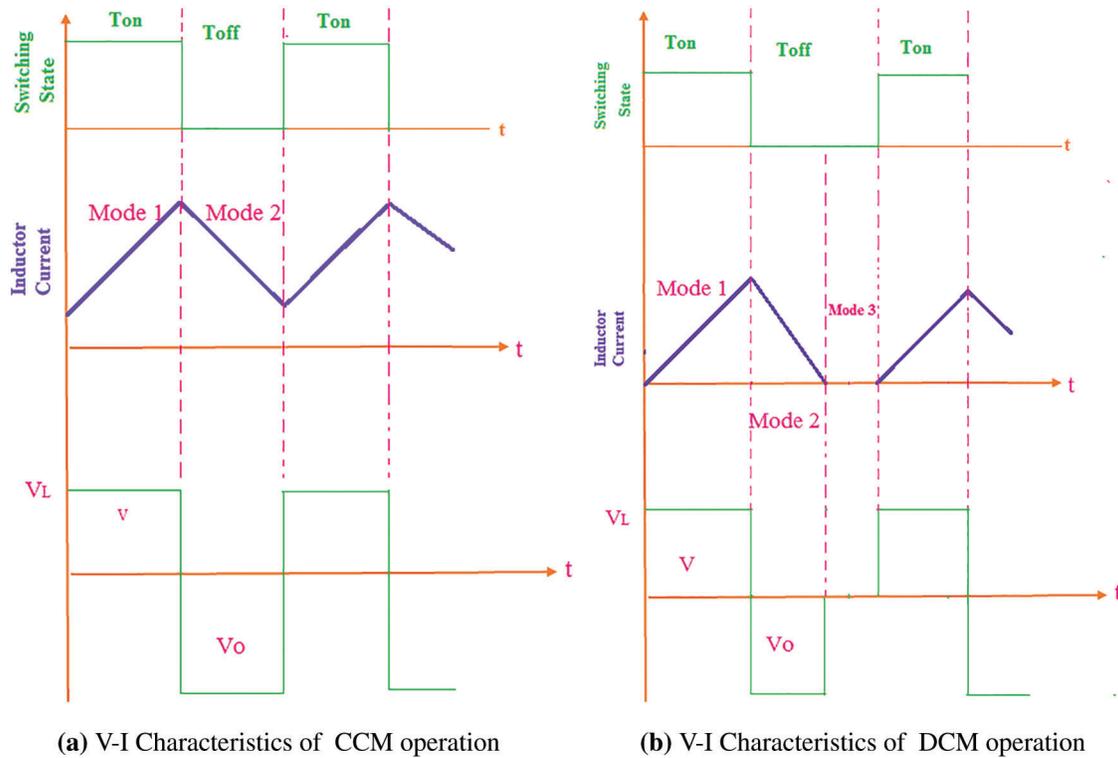
(a) V-I Characteristics of CCM operation

(b) V-I Characteristics of DCM operation

Figure 14: VI characteristics of voltage and current response

2.3 Optimization and Power Management Analysis of Converters Using Adaptive Nonlinear Sliding Mode Control Strategy

Power management is the main requirement of a power converter system. The strategy of the circuit to handle both source-side imbalances and load-side variations is adaptively optimized in the controller and executed to stabilize the overall system performance. This work proposes optimal control in an adaptive nonlinear sliding control approach involving individual parameter control arising due to nonlinearities. The new results depend on the traditional hypothesis of ideal control that permits the ongoing outcomes to unravel the framework issues. All the more explicitly, ANSM is utilized to discover arrangements that are good for compelling force the board with the unimportant loss of intensity.

ANSM-Algorithm Steps

Step1: Size of the populace (s) and repetitions (j) are initialized.

Step2: Select samples from general population, where $j = 1, 2, 3....$for different loads. Set the boundaries for the maximum number of repetitions.

Step3: Specify the ideal limit with the ultimate objective that assesses different loads with voltage modifications.

Step4: Compute the boundaries by considering the three facts (i) different load conditions ii) Input power factor. iii) Switching frequency and duty cycle of converters.

Step 5: Calculate the testing periods $Ti + 1$ based on the quality requirement

Step6: Based on the response of testing results, the error value is computed

$$\Delta s = Vout - e \tag{6}$$

Step 7: From the error value, the load's error rate is adjusted

$$L = L + \Delta \tag{7}$$

Step8: If the state of the movement of the issue isn't fulfilled, go to step3.

Step9: Upgrade the new adjustments of the individual loads in the general population freely.

Step10: If the error value is high, go to step3 and repeat the process

Step11: If the end outcome is met, fix the possible ideal plan in the request space.

The algorithm is developed for the ANSM control of the proposed DC-DC and AC-DC converters to manage the PWM signals of the switching devices of the converters. The following parameters are utilized to assess the performance of (i) Transient response in terms of Peak time, Peak overshoot and steady-state error, (ii) Total Harmonic Distortion (THD) and (iii) Overall System Efficiency.

3 Simulation Results and Discussion

The Proposed solar-based DC distribution system is implemented in the Simulink model and simulated in the MATLAB software. Two primary blocks make up the proposed simulation system: AC-DC converter and DC-DC converter. The DC load has a capacity of 2000 W and operates at 12, 24, and 48 V. Here we'll talk about the simulation circuit and the findings we got.

3.1 Performance Analysis of Solar DC-DC Converter

Below are the simulation results and performance analysis of a DC-DC converter with a solar source. The suggested solar-based DC-DC converter's Simulink model is illustrated in Fig. 15, and the

simulation parameters are provided in Tab. 1. In this work, the ANSM strategy generates the PWM and maintains the constant DC voltage.
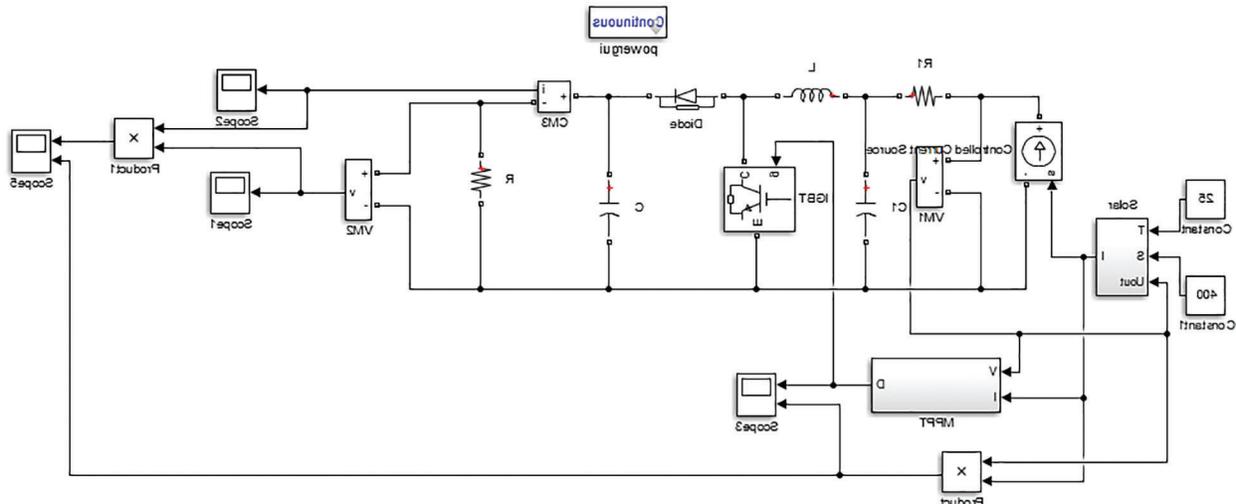
Figure 15: Simulink model solar with DC-DC converter

Fig. 16 shows the DC-DC Converter's input voltage from a solar source, with a DC input voltage of 200 V. The Voltage and current response of the switching device MOSFET is shown in Figs. 16b and 16c. respectively. The DC-DC Converter voltage response across the DC bus from the DC-DC converter is shown in Fig. 16d. The load voltage response and current response of the proposed system for a 48 V Permanent Magnet DC (PMDC) motor is shown in Figs. 16e and 16f.

3.2 Performance Analysis of AC-DC Converter

This section discusses the simulation results and performance analyses of the AC-DC converter. The suggested solar-based AC-DC converter's Simulink model is illustrated in Fig. 17, and the simulation parameters are provided in the Tabs. 2 and 3. The ANSM method is utilized to produce the PWM and keep the DC voltage constant in this study.

The input voltage and current of the AC-DC Converter are shown in Fig. 18a with an AC input voltage of 230 V. The Voltage and current response of the switching device MOSFET is shown in Figs. 18b and 18c. respectively. The inductor current response is shown in Fig. 18d. The AC-DC Converter voltage across the DC bus from the is shown in Fig. 18e. The proposed system's load voltage response and current response for a 48 V PMDC motor are shown in Figs. 18f and 18g.

3.3 Analysis of Total Harmonic Distortion

The THD analysis of the proposed converter is shown in Fig. 19. The proposed ANSM obtain the THD value of 3.31% only.

The performance analysis of control system parameters is discussed in Tab. 4 and Fig. 20. This comparison confirms that the proposed ANSM method achieves the best results, as compared with conventional methods.

(a) an Input Voltage from Solar Source

(b) The voltage response of MOSFET

(c) Current Response of MOSFET

(d) DC-DC converter voltage

(e) DC-DC converter with Load Voltage

(f) DC-DC converter with Load Current
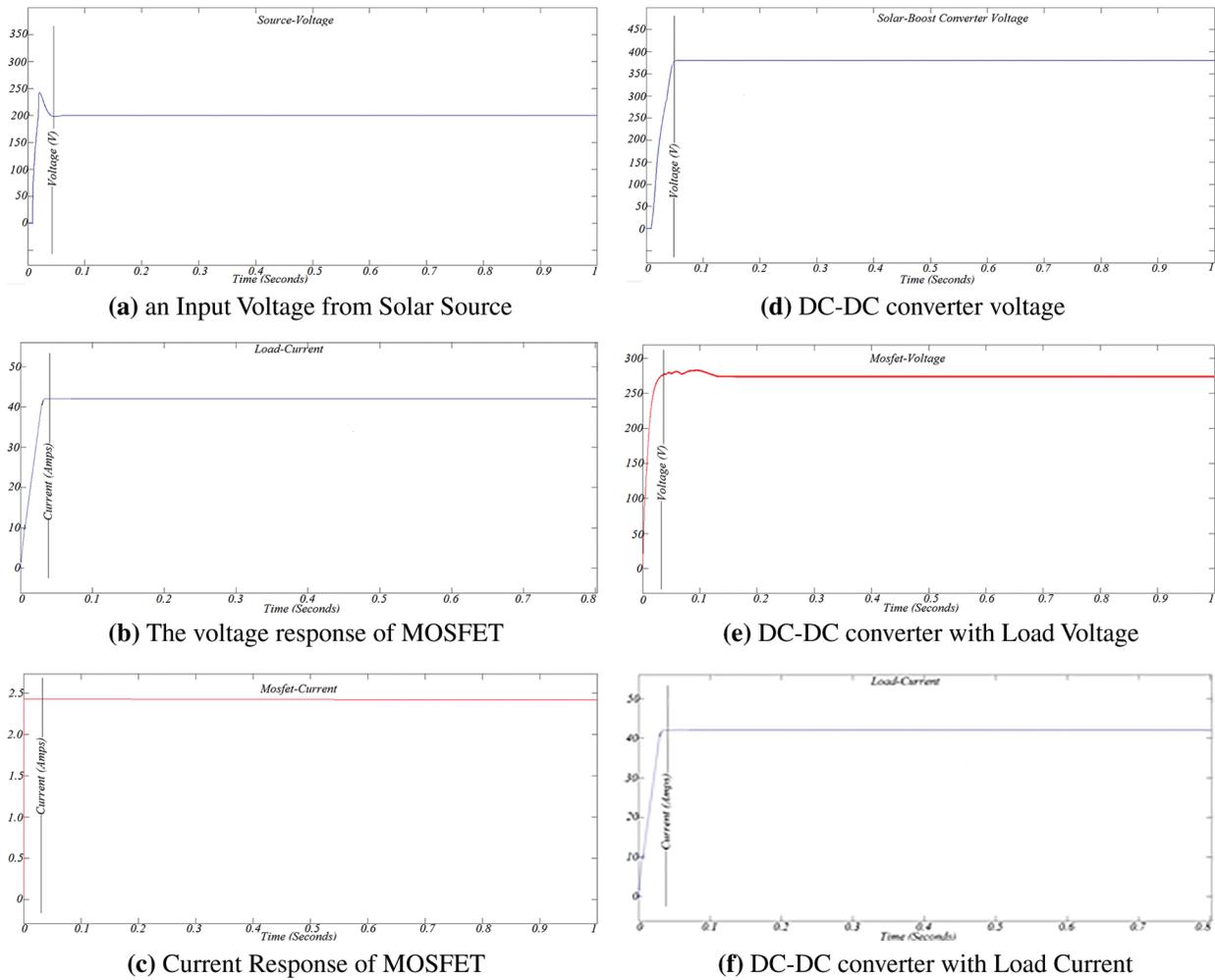
Figure 16: (a) An Input voltage from solar source (b). The voltage response of MOSFET (c) Current response of MOSFET (d). DC-DC converter voltage (e) DC-DC Converter with load voltage (f). DC-DC converter with load current
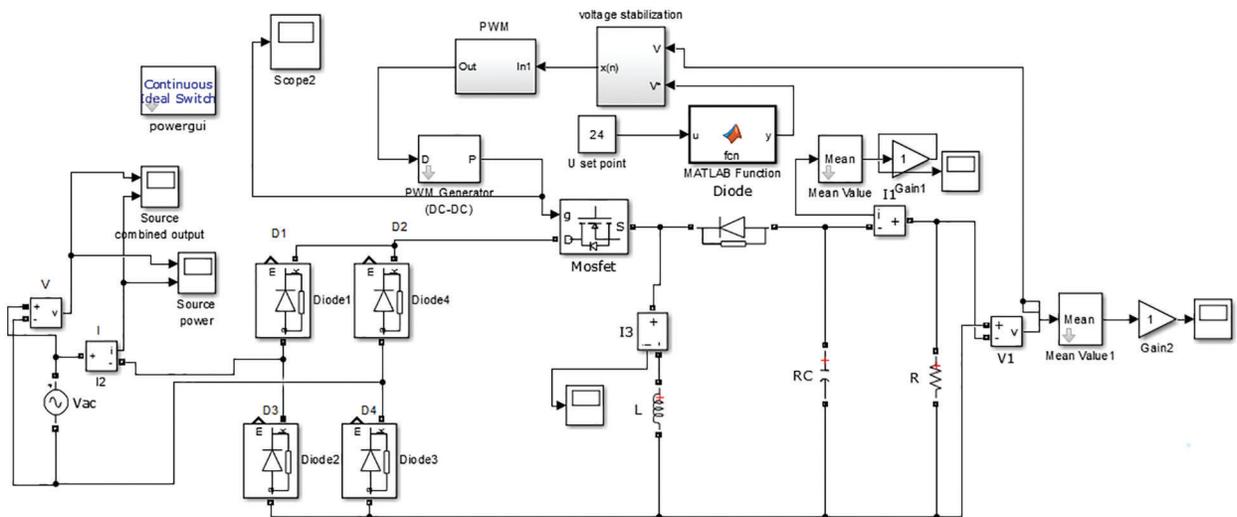
Figure 17: Simulink model of proposed AC-DC converter
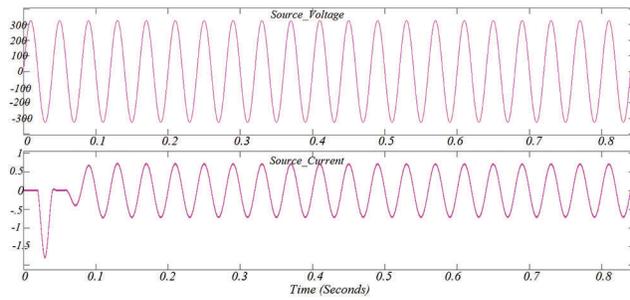
(a) an AC source voltage and source current
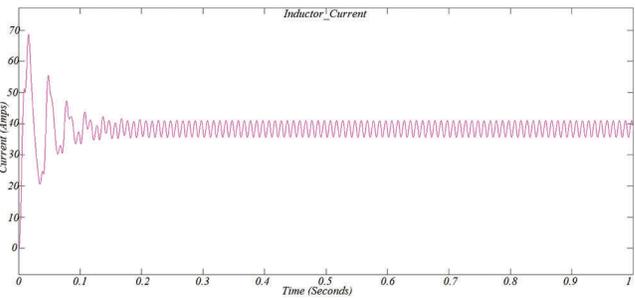
(d) Inductor Current Response
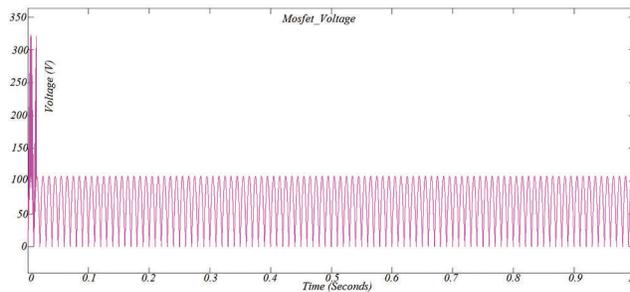
(b) Voltage Response of MOSFET
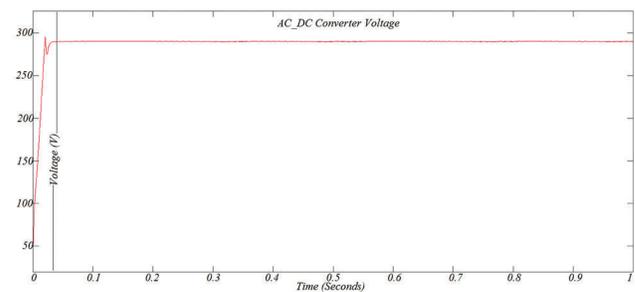
(e) AC-DC Converter Voltage
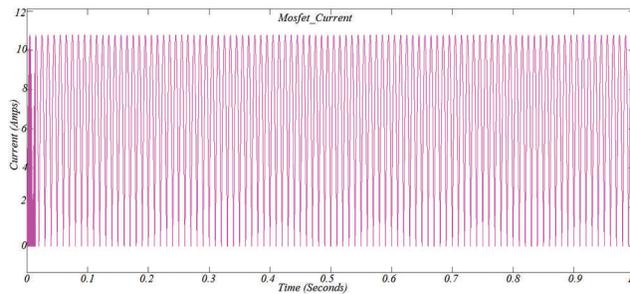
(c) Current Response of MOSFET
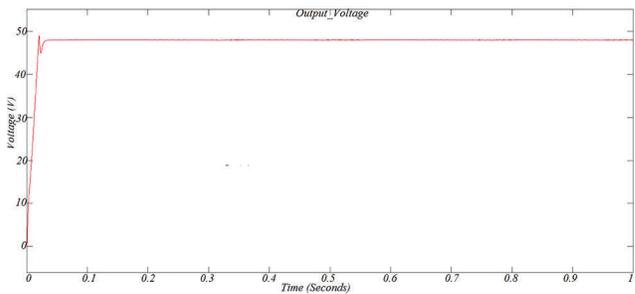
(f) Load Voltage of AC-DC Converter
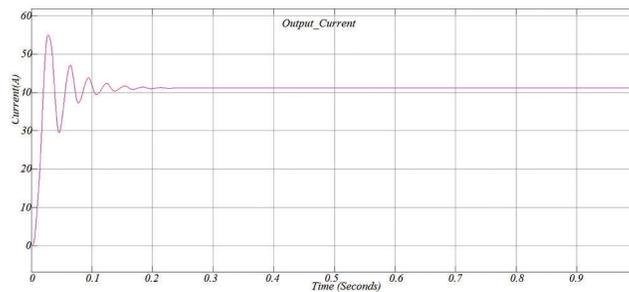
(g) Load Current of AC-DC converter

Figure 18: (a) An AC source voltage and source current (b) Voltage response of MOSFET (c) Current response of MOSFET (d) Inductor current response (e) AC-DC Converter voltage (f) Load voltage of AC-DC converter (g) Load current of AC-DC converter

Table 2: Simulation parameters of DC-DC converter with solar source

Software tool	MATLAB 2016a
Renewable power generation source	Solar PV Array
Total capacity	20 kWp
Indifference time	105–450 s
Startup power	40 W
Nominal voltage	635 Vdc
Short circuit current ISC (A)	24 A
Power conditioning unit parameters	
DC-DC Converter	380 V
Rated voltage	211 V
Resistance	0.02 Ohm
Inductance	10 μh
Capacitance	200 μf
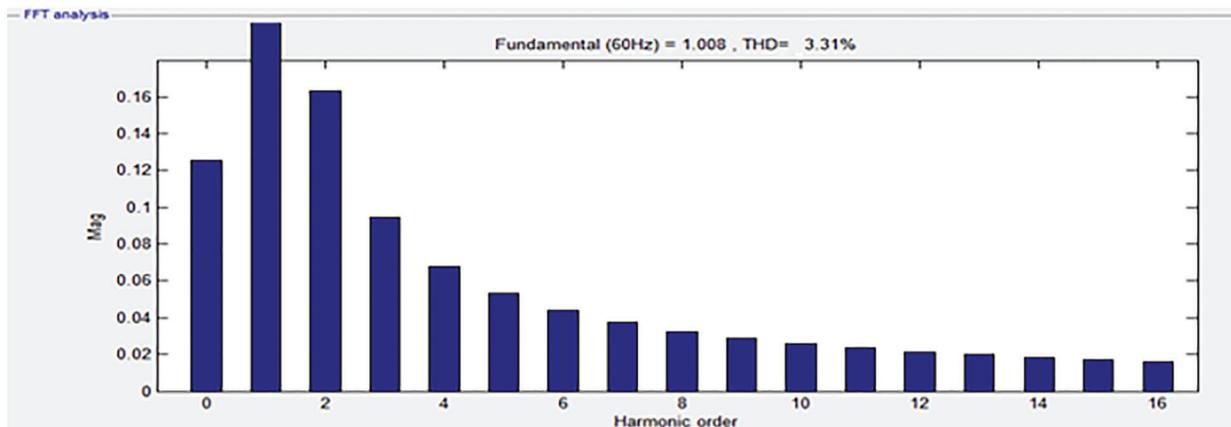
Figure 19: THD analysis for proposed system

Table 3: Simulation Parameters of AC-DC converter with Utility Source

Parameters	AC source	Vin (RMS)	DC Bus Volt	Maximum load	Switching frequency	Input power factor	Inductor	capacitor
Values	20 kVA	230 ± 10% V	380 V DC	2000 W	5 kHz	0.9715	100e-4 H	400e-8 Farad
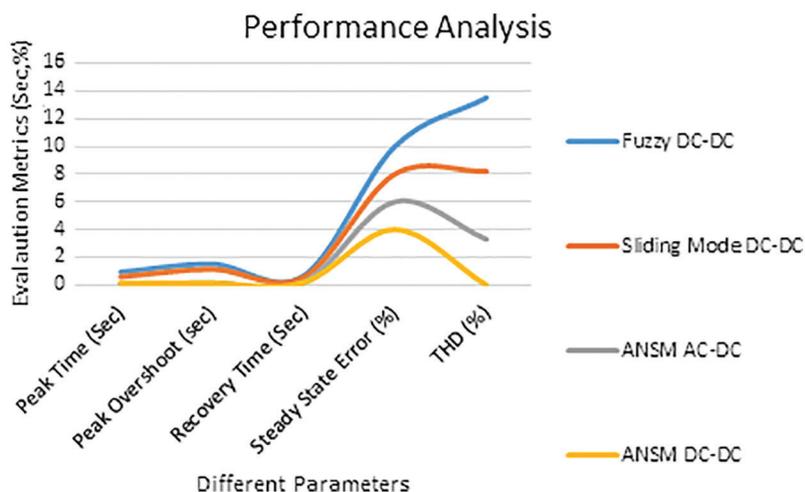
Figure 20: Performance analysis

Table 4: Performance analysis of Control system parameters

Methods		Peak time (sec)	Peak overshoot Time (sec)	Recovery time (sec)	Steady state error (%)	THD (%)
Fuzzy logic	*DC-DC*	0.9418	1.524	0.67	11	13.7
Sliding mode	*DC-DC*	0.6012	1.147	0.57	8	8.23
ANSM	*AC-DC*	0.122	0.152	0.21	6	3.3
	DC-DC	0.131	0.124	0.19	4	-

4 Conclusion

This work proposes an Adaptive Nonlinear Sliding Mode method of control that can drive the DC loads in commercial buildings from both AC and DC sources. The objective is to maintain constant DC bus voltage considering different operating conditions. The proposed system avails maximum utilization of PV sources. The DC bus voltage levels are monitored to coordinate the system's sources and storage and regulate the switching device under various operating situations. The suggested control techniques for integrating PV sources, utility sources, and energy storage in commercial buildings will be validated using system simulations. Compared with the existing system, the proposed method achieves the best results. For example, peak time is 012, peak overshoot time is 015 sec, recover time is 0.20 sec, the steady-state error is 6% and THD is 3.31%.In the Future, introduce deep learning methods to improve the power quality issues for solar-based commercial building application systems. The simulation results show that the suggested source design is more dependable and efficient than the current source configuration. Compared with the existing system, the proposed system achieves better results. For example, peak time is 0.12 sec, peak overshoot time is 0.15 sec, recovery time is 0.20 sec, the steady-state error is 6% and THD is 3.31%. Future neural networks with optimization methods will be involved to improve the power quality issues of the DC Distribution in commercial buildings.

Conflicts of Interest: The authors declare that they have no conflicts of interest to report regarding the present study.

References

[1] R. Mohd, M. Sharip, M. Ahmed. A. Haidar and C. Aaron Jimel, "Optimum configuration of solar PV topologies for DC micro grid," *International Journal of Photo Energy*, vol. 4, no. 23, pp. 13–26, 2019.

[2] R. Asensio, E. Simón-Martín, M. Borge-Diez, D. Blanes Peiró, J. Juan *et al.,* "Micro grids with energy storage systems as a means to increase power resilience: An application to office buildings," *Energy & Elsevier*, vol. 172, no. 4, pp. 1005–1015, 2019.

[3] K. Sundareswaran, K. Ark Kumar, K. Raman Venkateswaran and P. P. Sathya, "Solar photovoltaic fed dual input LED lighting system with constant illumination control," *Frontiers in Energy*, vol. 14, no. 26, pp. 213–231, 2016.

[4] K. Lai, E. Muir, S. Erboy Ruff and Z. Yasemin, "Off-grid appliance performance testing: Results and trends for early-stage market development," *Energy Efficiency*, vol. 13, no. 2, pp. 232–244, 2019.

[5] S. Vishwanath, A. Chandan, V. Saurav and L. Kumar, "An IoT based data driven pre-cooling solution for electricity cost savings in commercial buildings," *IEEE Internet of Things Journal*, vol. 12, no. 23, pp. 1–1, 2019.

[6] G. Arunkumar Devaraj, P. Elangovan, P. Sanjeevi kumar, H. Nielsen and L. Peter, "DC grid for domestic electrification," *Energies*, vol. 24, no. 9, pp. 236249, 2019.

[7] E. Gelani, H. Dastgeer, F. Siraj, K. Nasir, M. Niazi *et al.,* "Efficiency comparison of AC and DC distribution networks for modern residential localities," *Applied Sciences*, vol. 9, no. 4, pp. 213–226, 2019.

[8] J. Kitson, S. J. Williamson, P. W. Harper Mcmahon, C. G. Rosenberg, M. Tierney *et al.,* "Modelling of an expandable, reconfigurable, renewable DC micro grid for off-grid communities," *Energy*, vol. 06, no. 219, pp. 415–429, 2018.

[9] S. Comello, L. Reichelstein and S. Sahoo, "The road ahead for solar PV power-renewable and sustainable," *Energy Reviews*, vol. 92, no. 8, pp. 744–756, 2018.

[10] S. Chuang, K. Hsing-Lung Den, W. Iskandar, L. Liao and P. Hsuan. "The relationship between electricity emission factor and renewable energy certificate: The free rider and outsider effect," *Sustainable Environment Research*, vol. 28, no. 18, pp. 513–531, 2018.

[11] Y. Zhou and X. Chen, "Mechanism of CO_2 emission reduction by global energy," *Interconnection Global Energy Interconnection*, vol. 1, no. 4, pp. 409–419. 2018.

[12] X. Zandi and Z. Mazinan, "Maximum power point tracking of the solar power plants in shadow mode through artificial neural network," *Complex & Intelligent Systems*, vol. 19, no. 13, pp. 13–29, 2019.

[13] K. Mossad, I. Mohamed, O. abed el-Raouf, M. Alahmar and Z. Fahd, "Maximum power point tracking of PV system based cuckoo search algorithm; review and comparison," *Energy Procedia*, vol. 4, no. 13, pp. 117–126. 2019.

[14] K. Schuss, V. Christian and L. Fabritius, "Moving photovoltaic installations: Impacts of the sampling rate on maximum power point tracking algorithms," *IEEE Transactions on Instrumentation and Measurement*, vol. 12, no, 5, pp. 1–9, 2019.

[15] N. Krishnaraj, M. Elhoseny, E. Laxmi Lydia, K. Shankar and O. ALDabbas, "An efficient radix trie-based semantic visual indexing model for large-scale image retrieval in cloud environment," *Software: Practice and Experience*, vol. 51, no. 3, pp. 489–502, 2021.

[16] L. Anzalchi and A. Sarwat, "Overview of technical specifications for grid-connected photovoltaic systems," *Energy Convers*, vol. 12, no. 15, pp. 2312–327, 2017.

[17] J. H. Jo, M. Aldeman and R. D. G. Loomis, "Optimum penetration of regional utility-scale renewable energy systems," *Renewable Energy*, vol. 2, no. 118, pp. 328–334, 2018.

[18] C. Vezzoli, "Distributed/decentralized renewable energy systems. in: Designing sustainable energy for all green energy and technology," *Springer*, vol. 15, no. 4, pp. 12–31, 2018.

[19] S. Cheng, K. Lefeng Zhang, L. Zhiyi Jiang, H. Tao, Y. Wang *et al.,* "Local energy management and optimization: A novel energy universal service bus system based on energy internet technologies," *Energies*, vol. 4, no. 15, pp. 322–341, 2018.

[20] J. L. Hernandez, R. Sanz, A. Corredera, R. Palomar and I. Lacave, "A Fuzzy-based building energy management system for energy efficiency," *Buildings*, vol. 8, no. 2, pp. 326–339, 2018.

[21] K. Rehman, A. Ashraf, M. Bhatti and Z. Aamer, "Fixed frequency sliding mode control of power converters for improved dynamic response in DC micro-grids," *Energies*, vol. 11, no. 16, pp. 31–45, 2018.

[22] N. Krishnaraj, B. Sivakumar, R. Kuppusamy, Y. Teekaraman and A. R. Thelkar, "Design of automated deep learning based fusion model for copy-move image forgery detection," *Computational Intelligence and Neuroscience*, vol. 2022, no. 8501738, pp. 1–13, 2022.

[23] R. Saravanakumar, N. Krishnaraj, S. Venkatraman, B. Sivakumar, S. Prasanna *et al.*, "Hierarchical symbolic analysis and particle swarm optimization based fault diagnosis model for rotating machineries with deep neural networks," *Measurement*, vol. 171, no. 108771, pp. 1–12, 2021.